论著·临床医学

基于磁共振DSC-PWI构建的肿瘤血管生境对胶质母细胞瘤和单发脑转移瘤鉴别诊断效能的研究

李 轩[1],王瀚苇[1,2],曾琳岚[1,2],赵咪咪[1,2],封 铃[1,2],谢 欢[1,2],冉启胜[1,2],马 强[3],王舒楠[1,2] [1]陆军军医大学大坪医院放射科,重庆;[2]重庆市影像学与核医学临床研究中心,重庆;[3]陆军军医大学大坪医院病理科,重庆

[**摘要**] **目的** 探讨基于磁共振动态磁敏感对比增强灌注加权成像(dynamic susceptibility contrast-enhanced perfusion weighted imaging,DSC-PWI)构建的肿瘤血管生境特征参数对初诊胶质母细胞瘤(Glioblastoma,GBM)和单发脑转移瘤(solitary brain metastasis,SBM)的鉴别诊断价值。**方法** 采用病例对照研究方法,回顾性分析中国人民解放军陆军特色医学中心放射科2019年1月至2025年3月期间经术后病理证实或临床综合诊断的109例恶性脑肿瘤患者(其中胶质母细胞瘤57例,单发脑转移瘤52例)的影像学资料。基于DSC-PWI图像,采用血流动力学组织特征(hemodynamic tissue signature,HTS)法分割病灶并构建4种肿瘤血管生境,分别为增强区高血管生境(high angiogenic tumor,HAT)、增强区低血管生境(low angiogenic tumor,LAT)、肿瘤浸润性水肿(potentially infiltrated peripheral edema,IPE)和瘤周血管源性水肿区(vasogenic peripheral edema,VPE)。计算各生境区域体积参数和血流参数,包括各生境区域体积、肿瘤核心体积、瘤周水肿体积和相对脑血容量值(relative cerebral blood volume,rCBV),比较两组患者基线资料和生境特征参数,绘制受试者工作特征(receiver operating characteristic,ROC)曲线评估鉴别诊断效能。运用Pearson相关性分析判断各生境特征参数间的相关性以量化各生境间的空间相互作用。**结果** 胶质母细胞瘤组HAT、LAT、IPE、VPE四种生境区域的rCBV中位值($rCBV_{median}$)分别为6.143±1.687(95%*CI*:5.695~6.591)、3.249±0.988(95%*CI*:2.987~3.511)、1.913(1.578,2.588)(95%*CI*:1.794~2.110)、0.836(0.676,1.110)(95%*CI*:0.710~0.949)。均高于单发脑转移瘤组的$rCBV_{median}$值[4.634±1.647(95%*CI*:4.175~5.092)、2.255±0.807(95%*CI*:2.031~2.480)、1.291(1.022,1.767)(95%*CI*:1.125~1.677)、0.600(0.459,0.742)(95%*CI*:0.519~0.682)](*P*<0.001)。经ROC曲线分析,LAT中$rCBV_{median}$值具有良好的鉴别诊断效能,其AUC值为0.792(95%*CI*:0.704~0.864),最佳截断值为2.660(敏感性:75.44%,特异性:78.85%),(*P*<0.001)。胶质母细胞瘤组IPE体积与瘤周体积比($V_{(IPE)}/V_{(P)}$)为0.216(0.101,0.351)(95%*CI*:0.165~0.267),高于单发脑转移瘤组0.079(0.055,0.153)(95%*CI*:0.066~0.102)(*P*<0.001)。经ROC曲线分析,$V_{(IPE)}/V_{(P)}$具有良好的鉴别诊断效能,AUC值为0.765(95%*CI*:0.674~0.840),最佳截断值为0.122(敏感性:71.93%,特异性:73.08%),(*P*<0.001)。Pearson相关性分析显示,GBM组IPE-$rCBV_{median}$和VPE-$rCBV_{median}$与HAT-$rCBV_{median}$间的相关系数分别为0.620(*P*<0.01)、0.283(*P*=0.033),呈显著正相关。**结论** 基于磁共振DSC-PWI构建的肿瘤血管生境特征参数在初诊GBM和SBM中差异明显,其体积特征参数$V_{(IPE)}/V_{(P)}$和血流特征参数LAT-$rCBV_{median}$均具有较好的鉴别诊断效能,可作为两者鉴别诊断的影像学标记。

[**关键词**] 胶质母细胞瘤;单发脑转移瘤;磁共振成像;生境成像

[**中图法分类号**] R445.2;R447;R739.41 [**文献标志码**] A

[**基金项目**] 重庆市科卫联合医学科研项目(2025QNXM014)

[**通信作者**] 王舒楠,E-mail:wangshunan@tmmu.edu.cn

2097-0927/Copyright © 2025,陆军军医大学(第三军医大学)。这篇开放获取文章遵循CC BY许可协议(https://creativecommons.org/licenses/by/4.0/)

引用格式:李轩,王瀚苇,曾琳岚,等. 基于磁共振DSC-PWI构建的肿瘤血管生境对胶质母细胞瘤和单发脑转移瘤鉴别诊断效能的研究[J]. 陆军军医大学学报,2025,47(24):3102-3111. DOI:10.16016/j.2097-0927.202509101.

Citation:LI X,WANG H W,ZENG L L,*et al*. Differential diagnostic efficacy of tumor vascular habitats based on DSC-PWI between glioblastoma and solitary metastatic brain tumors[J]. J Army Med Univ,2025,47(24):3102-3111. DOI:10.16016/j.2097-0927.202509101.

Differential diagnostic efficacy of tumor vascular habitats based on DSC-PWI between glioblastoma and solitary metastatic brain tumors

LI Xuan[1], WANG Hanwei[1,2], ZENG Linlan[1,2], ZHAO Mimi[1,2], FENG Ling[1,2], XIE Huan[1,2], RAN Qisheng[1,2], MA Qiang[3], WANG Shunan[1,2] [1]Department of Radiology; [2]Chongqing Clinical Research Centre of Imaging and Nuclear Medicine, Chongqing; [3]Department of Pathology, Daping Hospital, Army Medical University, Chongqing, China

[**Abstract**] Objective To investigate the value of tumor vascular habitat characteristic parameters constructed based on dynamic susceptibility contrast-enhanced perfusion-weighted imaging (DSC-PWI) in differentiating between newly diagnosed glioblastoma (GBM) and solitary brain metastasis (SBM). Methods A case-control study design was adopted to analyze the imaging data of 109 patients with malignant brain tumors (including 57 cases of GBM and 52 cases of SBM) confirmed by postoperative pathology or comprehensive clinical diagnosis retrospectively collected from Department of Radiology of Daping Hospital between January 2019 and March 2025. Based on DSC-PWI images, hemodynamic tissue signature (HTS) was used to segment the lesions and construct 4 tumor vascular habitats, that is, high angiogenic tumor (HAT), low angiogenic tumor (LAT), potentially infiltrated peripheral edema (IPE), and vasogenic peripheral edema (VPE). Volume parameters and blood flow parameters for each habitat region were calculated, including volume of each habitat region, tumor core volume, peritumoral edema volume, and relative cerebral blood volume (rCBV). Baseline data and habitat characteristic parameters were compared between the 2 groups. Receiver operating characteristic (ROC) curves were drawn to evaluate the differential diagnostic efficacy. Pearson correlation analysis was performed to assess the correlations among habitat characteristic parameters to quantify the spatial interactions between habitats. Results In the GBM group, the median rCBV ($rCBV_{median}$) at HAT, LAT, IPE, and VPE habitats were 6.143±1.687 (95%*CI*: 5.695~6.591), 3.249±0.988 (95%*CI*: 2.987~3.511), 1.913 (1.578, 2.588) (95%*CI*: 1.794~2.110) and 0.836 (0.676, 1.110) (95%*CI*: 0.710~0.949), respectively. These values were all significantly higher than the $rCBV_{median}$ at above habitats in the SBM group [4.634±1.647 (95%*CI*: 4.175~5.092), 2.255±0.807 (95%*CI*: 2.031~2.480), 1.291 (1.022, 1.767) (95%*CI*: 1.125~1.677), 0.600 (0.459, 0.742) (95%*CI*: 0.519~0.682); $P<0.001$]. ROC curve analysis showed that the $rCBV_{median}$ at LAT habitat had good diagnostic efficacy for differentiation, with an AUC value of 0.792 (95%*CI*: 0.704~0.864) ($P<0.001$). The optimal cutoff value of $rCBV_{median}$ at LAT habitat was 2.660 (sensitivity: 75.44%, specificity: 78.85%). The ratio of IPE volume to peritumoral volume ($V_{(IPE)}/V_{(P)}$) in the GBM group was 0.216 (0.101, 0.351) (95%*CI*: 0.165~0.267), notably higher than that in the SBM group [0.079 (0.055, 0.153) (95%*CI*: 0.066~0.102), $P<0.001$]. ROC curve analysis indicated that $V_{(IPE)}/V_{(P)}$ ratio had good diagnostic efficacy, with an AUC value of 0.765 (95%*CI*: 0.674~0.840). The optimal cutoff value of the ratio was 0.122 (sensitivity: 71.93%, specificity: 73.08%). Pearson correlation analysis suggested that in the GBM group, the correlation coefficients between IPE-$rCBV_{median}$ and HAT-$rCBV_{median}$, and between VPE-$rCBV_{median}$ and HAT-$rCBV_{median}$ were 0.620 ($P<0.01$) and 0.283 ($P=0.033$), respectively, indicating significant positive correlations. Conclusion DSC-PWI-based vascular habitat characteristic parameters show significant differences between newly diagnosed GBM and SBM. Both the volumetric parameter $V_{(IPE)}/V_{(P)}$ ratio and the hemodynamic parameter LAT-$rCBV_{median}$ have good differential diagnostic efficacy, and can serve as imaging markers for distinguishing between GBM and SBM.

[**Key words**] glioblastoma; solitary brain metastasis; magnetic resonance imaging; habitat imaging

Supported by the Joint Medical Research Project of Chongqing Science and Technology Commission and Chongqing Health Commission (2025QNXM014).

Corresponding author: WANG Shunan, E-mail: wangshunan@tmmu.edu.cn

胶质母细胞瘤(Glioblastoma,GBM)和脑转移瘤(brain metastasis,BM)均是成人颅内常见的恶性肿瘤。两者的治疗方案存在较大差异,初诊的GBM通常进行最大范围安全切除并术后辅以化疗和放疗[1],而脑转移瘤则需根据病灶及患者的具体病情综合制定治疗方案[2]。因此,准确的术前鉴别诊断对治疗方案的制定有重要意义。

MRI是目前颅内肿瘤最重要的成像技术,但在常规MRI中,胶质母细胞瘤和脑转移瘤可表现相似的影像学表现,如环形强化并伴有广泛瘤周水肿等,且肿瘤内部均可出现囊变、坏死及出血等特征。特别是在缺乏原发肿瘤病史的单发脑转移瘤(solitary brain metastasis,SBM)病例中,两者更是难以准确诊断[3-4]。目前MRI多模态功能成像技术用于两者的鉴别诊断,如弥散成像、灌注成像及波谱成像等技术有助于两者的鉴别[5-6],但其临床应用价值仍有待进一步提高。血管生境成像是近年兴起的一项基于DSC-PWI的MRI处理技术,能够非侵入性聚类分割肿瘤内部具备特定图像特性的空间亚区域,定量分析肿瘤内部的细微影像差异,进而反映肿瘤血管微环境的空间异质性[7-8]。生境成像有望通过可视化和量化肿瘤微环境的空间异质性对GBM和SBM两类具有不同生物学性质的肿瘤进行鉴别,为术前精准影像诊断提供一种新方法。

因此,本研究拟针对GBM和SBM术前鉴别诊断困难这一临床问题,回顾性分析陆军特色医学中心放射科2019年1月至2025年3月期间经术后病理证实或临床综合诊断的175例GBM和SBM患者的临床及影像学资料。基于DSC-PWI构建肿瘤血管生境,可视化2类肿瘤血管微环境的空间异质性,定量分析包括体积参数和血流参数在内的生境特征差异,探讨肿瘤血管生境成像对GBM和SBM的术前鉴别诊断价值。

1 资料与方法

1.1 研究对象

本研究经中国人民解放军陆军特色医学中心伦理委员会批准[医研伦审(2025)第90号],且免除了患者的知情同意。采用病例对照研究方法,回顾性分析陆军特色医学中心放射科2019年1月至2025年3月期间经术后病理证实或临床综合诊断的175例GBM和SBM患者的临床及影像学资料。纳入标准如下:①经术后病理学证实的GBM;②经术后病理证实或临床综合诊断的SBM患者;③患者在治疗前1周内行颅脑MRI扫描。排除标准:①复发病例;②合并颅内其他病变;③年龄小于18岁;④MRI检查前行颅脑放化疗者;⑤MRI图像序列不全;⑥图像质量不佳或存在伪影。最终符合纳入及排除标准的GBM患者共57例,SBM患者共52例。纳排流程如图1。

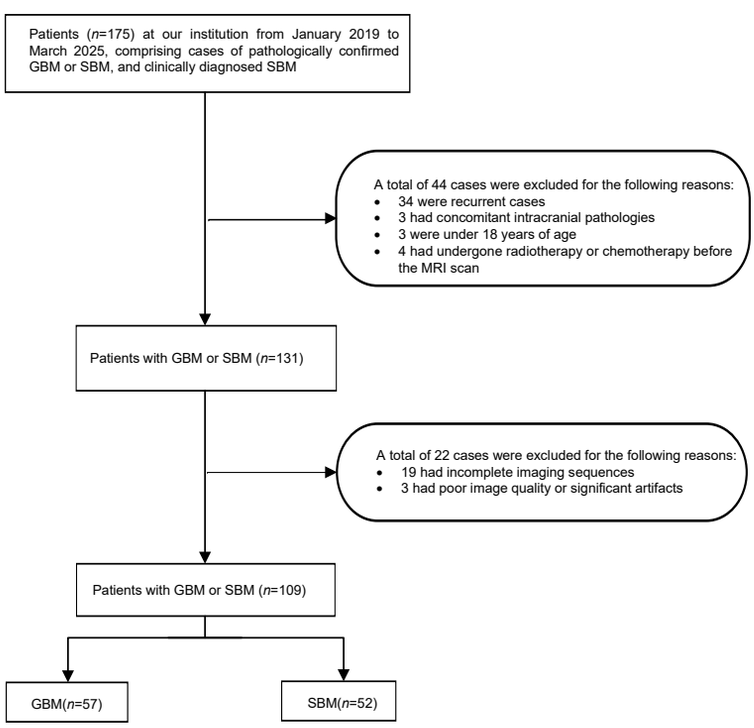


图1 临床病例纳排流程图

Figure 1 Flowchart of case inclusion and exclusion

1.2 检查方法

所有患者均采用Siemens Verio 3.0 T超导型磁共振扫描仪和8通道头颅线圈扫描。MRI扫描序列及参数包括:常规T1加权成像(T1 weighted imaging,T1WI)、T2加权成像(T2 weighted imaging,T2WI)、T2加权液体衰减反转恢复序列(T2 weighted fluid attenuation inversion recovery,FLAIR)序列、增强T1加权成像(contrast enhanced T1 weighted imaging,CE-T1WI)及DSC-PWI。各序列扫描参数如表1。CE-T1WI和DSC-PWI均使用对比剂钆喷替酸葡甲胺(北京北陆药业股份有限公司)经静脉团注,剂量均为0.2 mL/kg,流速分别为3、4 mL/s。

1.3 图像处理

纳入研究的患者术前MRI图像均以DICOM格式从本院PACS系统导出。采用ITK-SNAP 4.2手动设置感兴趣区域容积(volumes of interest,VOI),包含肿瘤核心及瘤周水肿区域。将CE-T1WI图像中肿瘤强化区域定义为肿瘤核心区(Tumor core),包括肿瘤囊变、坏死和出血部分;将强化区域以外、FLAIR图像上高信号水肿区域定义为瘤周水肿区(Peritumoral)。基于ONCOhabitats在线系统(www.oncohabitats.upv.es)构建肿瘤血管生境,获得增强区高血管生境(high angiogenic tumor,HAT)、增强区低血管生境(low angiogenic tumor,LAT)、肿瘤浸润性水肿(potentially infiltrated peripheral edema,IPE)和瘤周血管源性水肿区(vasogenic peripheral edema,VPE)4种生境区域,处理流程见图2。

1.4 研究质量控制及研究资料采集

将原始图像导入Siemens Syngo工作站,两名神经影像医师在双盲条件下独立进行MRI肿瘤常规影像

表1 MRI设备扫描参数

Table 1 MRI scan parameters

Scanning sequence	Repetition time (ms)	Echo time (ms)	Inversion time (ms)	Slice thickness (mm)	Matrix	Field of view (mm)	Flip angle
T1WI	268	2.67	-	5	320×256	230×230	90°
T2WI	3 800	96	-	5	320×320	240×240	150°
FLAIR	8 000	94	2 370	5	256×256	230×230	150°
CE-T1WI	250	2.67	-	5	320×256	230×230	90°
DSC-PWI	1 500	30	-	5	128×128	240×240	60°

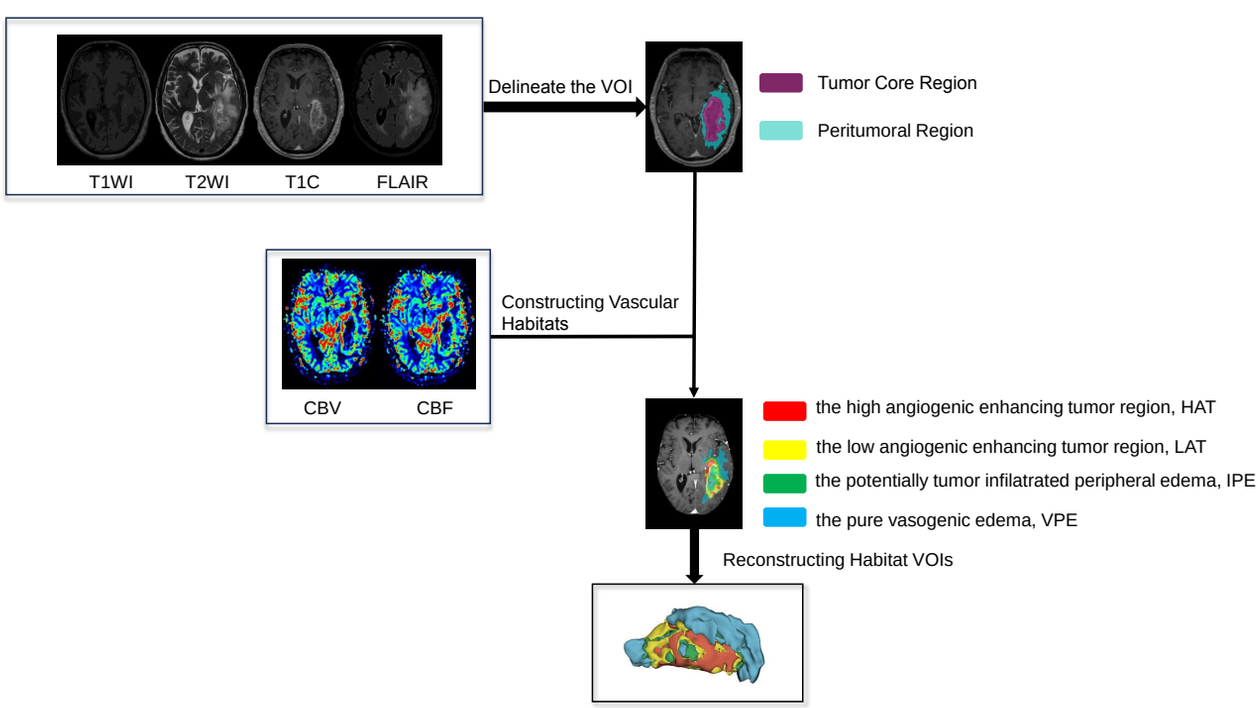


图2 肿瘤生境处理流程图

Figure 2 Flowchart of tumor habitat processing

征象分析,通过ITK-SNAP 4.2软件手动分割肿瘤后计算各分割体积获得肿瘤核心体积($V_{(T)}$)、瘤周水肿体积($V_{(P)}$)及各生境区域体积。两位医师在分析过程中若存在分歧,经讨论后达成一致,以确保分析的准确性和可靠性。采用Kappa检验评估2名医生对MRI肿瘤常规影像征象分析和肿瘤分割的一致性。Kappa值在0.75~1.00之间表示一致性较高。

常规影像征象包括强化方式、瘤周水肿、肿瘤出血、坏死及中线移位。强化方式分为环形强化和片状强化,环形强化为CE-T1WI中不均匀的围绕肿瘤中央非强化区域的闭合强化环,片状强化为CE-T1WI中不规则的斑片状或地图状强化区域。肿瘤生境特征参数包括体积参数和血流参数,体积参数为各生境区域体积与肿瘤核心或瘤周水肿体积比。血流参数为4类生境区域的rCBV值,使用MATLAB R2024a 24.1软件通过γ-变量曲线下面积(Area Under the γ-Variate Curve,AUCγ)的数值积分计算获得。

1.5 统计学分析

采用SPSS 27.0、MedCalc 20.100软件及R 4.4.2软件进行统计学分析。本研究为回顾性分析,共纳入109例患者,其中GBM组57例,SBM组52例。以LAT-$rCBV_{median}$作为主要结局指标进行事后把握度分析,计算Cohen's d效应值为1.097。在α=0.05(双侧)条件下,本样本量检测该差异的统计学把握度为>99%,表明当前样本量对主要结局指标具有极强的检验效能。符合正态分布的连续型变量以$\bar{x}\pm s$表示,不符合正态分布的连续型变量以$M(P_{25},P_{75})$表示。计数资料以频数(n)和率(%)表示。根据计量资料是否满足正态分布及方差齐性,对GBM与SBM的生境特征参数进行独立样本t检验或非参数Mann-Whitney U检验。计数资料的比较采用χ^2检验或Fisher精确概率检验。通过受试者工作特征(receiver operating characteristic,ROC)曲线下面积(area under the curve,AUC)、敏感性、特异性评估生境定量参数鉴别2类肿瘤的效能。采用Pearson相关性分析评价各生境特征参数的相关性。所有假设均为双侧检验,以P<0.05为差异有统计学意义。

2 结果

2.1 患者临床资料

根据纳入及排除标准,最终纳入GBM患者57例,其中男性36例,女性21例,平均年龄(55.82±12.98)岁;SBM患者52例,男性26例,女性26例,平均年龄(58.62±8.08)岁。2名医师对MRI肿瘤常规影像征象进行独立分析,Kappa检验显示MRI肿瘤常规影像特征在观察者间具有较高一致性,Kappa值为0.810~1.000(P<0.001)。两组患者在年龄、性别、瘤周水肿、瘤内出血、坏死及中线移位等特征之间,差异均无统计学意义(P>0.05)。GBM与SBM在病变部位和强化方式上存在显著性差异(P<0.001、P=0.002)。病变部位上,GBM以额叶(31.58%)、颞叶(33.33%)为主,SBM以枕叶(30.77%)、顶叶(28.85%)为主;强化方式上,GBM以环形强化为主(75.44%),SBM以片状强化为主(53.85%)。

表2 患者一般临床资料及影像征象比较[n(%),$\bar{x}\pm s$]

Table 2 Comparison of baseline clinical and imaging characteristics of the patients [n(%),$\bar{x}\pm s$]

Clinical data	GBM(n=57)	SBM(n=52)	$t/\chi^2/Z$	P
Age (years)	55.82±12.98	58.62±8.08	−0.792	0.428
Gender			1.919	0.166
Male	36(63.16)	26(50.00)		
Female	21(36.84)	26(50.00)		
Lesion sites			25.198	<0.001
Frontal lobe	18(31.58)	5(9.62)		
Temporal lobe	19(33.33)	7(13.46)		
Parietal lobe	11(19.30)	15(28.85)		
Occipital lobe	2(3.51)	16(30.77)		
Other locations	7(12.28)	9(17.31)		
Enhancement pattern			9.846	0.002
Ring-shaped enhancement	43(75.44)	24(46.15)		
Patchy enhancement	14(24.56)	28(53.85)		
Peritumoral edema			0.000	1.000
Yes	55(96.49)	50(96.15)		
No	2(3.51)	2(3.85)		
Hemorrhage			0.573	0.449
Yes	51(89.47)	44(84.62)		
No	6(10.52)	8(15.38)		
Necrosis			0.842	0.364
Yes	55(96.49)	47(90.38)		
No	2(3.51)	5(9.62)		
Midline shift			1.406	0.236
Yes	38(66.67)	40(76.92)		
No	19(33.33)	12(23.08)		

Other Lesion sites: Locations outside the frontal, temporal, parietal, and occipital lobes where the main tumor is situated, such as deep cerebral structures, infratentorial regions, and others. Levene's test revealed heterogeneity of variances in age, between the groups; Accordingly, Welch's t-test (the corrected t-test for unequal variances) was employed. The corrected P value was 0.428

2.2 GBM和SBM组生境体积参数的比较

GBM组HAT、LAT体积与肿瘤核心体积比$V_{(HAT)}/V_{(T)}$,$V_{(LAT)}/V_{(T)}$分别为0.298(0.223,0.374)、0.465(0.407,0.595)。IPE、VPE体积与瘤周体积比$V_{(IPE)}/V_{(P)}$,$V_{(VPE)}/V_{(P)}$分别为0.216(0.101,0.331)、0.558(0.477,0.630)。SBM组$V_{(HAT)}/V_{(T)}$、$V_{(LAT)}/V_{(T)}$ $V_{(IPE)}/V_{(P)}$和$V_{(VPE)}/V_{(P)}$四个值分别为0.323(0.203,0.454)、0.508(0.387,0.657)、0.079(0.055,0.153)、0.522(0.383,0.604)。仅GBM组$V_{(IPE)}/V_{(P)}$明显高于SBM组,差异具有统计学意义(P<0.01),而其他区域未表现出明显差异(P>0.05)(图3)。

2.3 GBM和SBM生境血流参数的比较

比较2种肿瘤各生境区域的生境血流参数(图4)。GBM组在HAT、LAT、IPE、VPE四种生境区域中的$rCBV_{median}$分别为6.143±1.687、3.249±0.988、1.913(1.578,2.588)、0.836(0.676,1.110)。SBM组在HAT、LAT、IPE、VPE中的$rCBV_{median}$分别为4.634±1.647、2.255±0.807、1.291(1.022,1.767)、0.600(0.459,0.742)。GBM组在HAT、LAT、IPE及VPE中的$rCBV_{median}$均显著高于SBM组(P<0.001)。

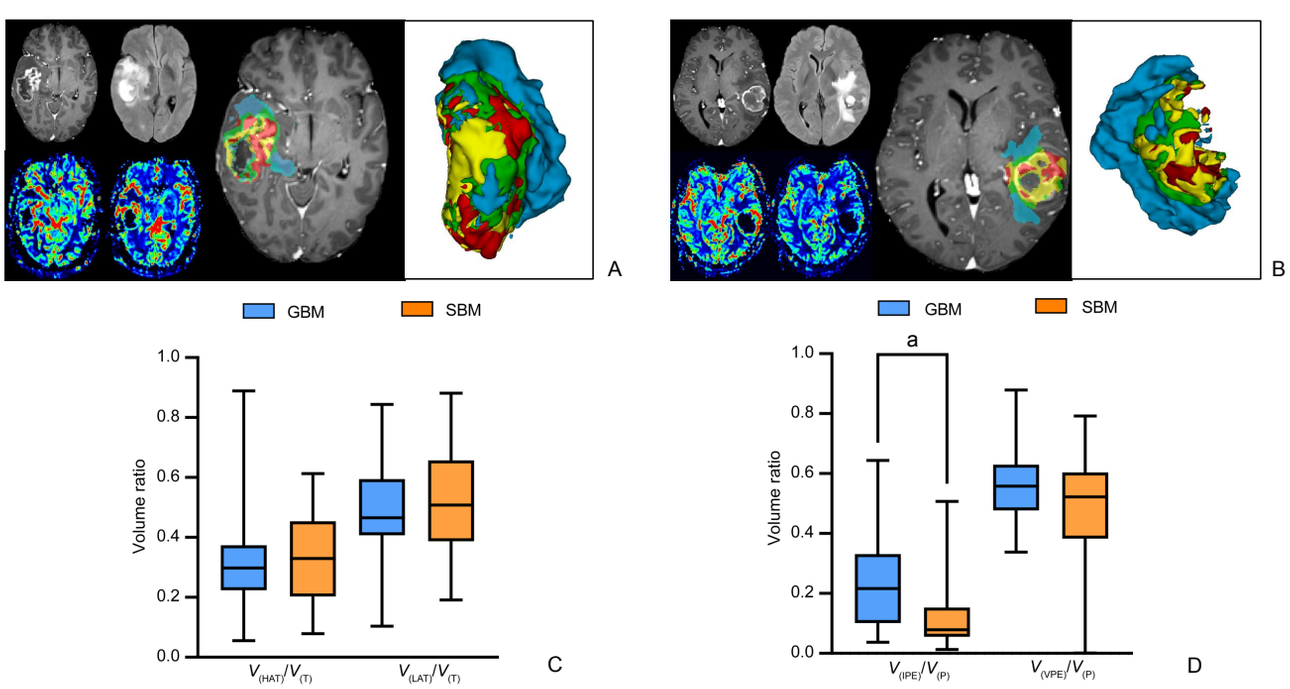
2.4 生境特征参数在鉴别GBM与SBM的诊断效能分析

对四种生境区域的体积参数和血流参数分别绘制ROC曲线分析(图5),具体诊断效能见表3。

生境体积参数在鉴别GBM和SBM中,仅$V_{(IPE)}/V_{(P)}$有显著意义,AUC值为0.765(95%*CI*:0.674~0.840),最佳截断值为0.122(敏感性:71.93%,特异性:73.08%)。生境血流参数中,LAT中的$rCBV_{median}$值在鉴别GBM和SBM中具有最佳诊断效能,其AUC值为0.792(95%CI:0.704~0.864),最佳截断值为2.660(敏感性:75.44%,特异性:78.85%)。

2.5 GBM和SBM组各生境区域作用的比较

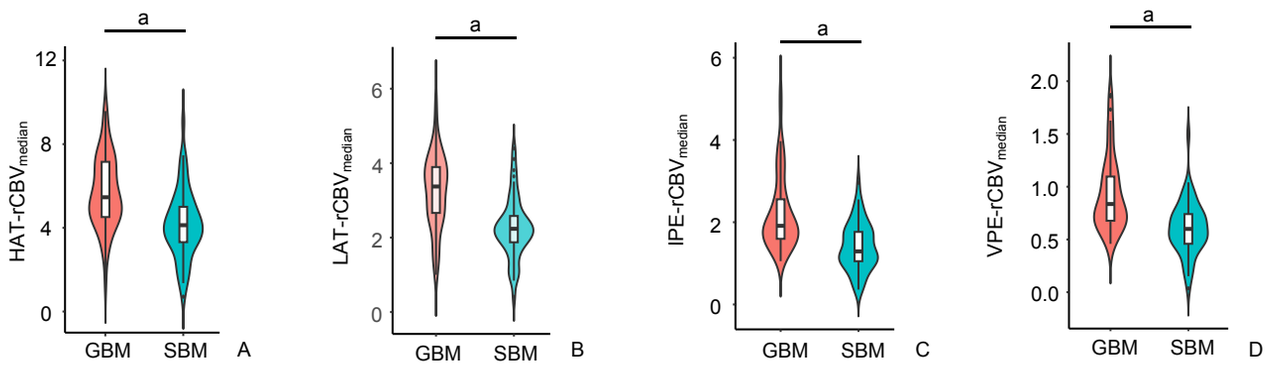
采用Pearson相关性分析方法,对GBM与SBM的四个生境区域的生境血流参数进行了相关性研究,并通过空间相互作用矩阵量化各生境区域相互作用(图6)。结果显示,GBM组IPE-$rCBV_{median}$和VPE-$rCBV_{median}$与



A: Conventional imaging and vascular habitat segmentation regions of a 49-year-old male patient with GBM. B: Conventional imaging and vascular habitat segmentation regions of a 48-year-old female patient with brain metastasis from intestinal adenocarcinoma. There are CE-T1WI, T2WI-FLAIR, CBV, CBF, vascular habitat segmentation images, and their 3D representations. Four colors represent 4 distinct habitat regions. C, D: Box plots comparing the habitat volume parameters of the GBM group and the SBM group, respectively

图3 GBM和SBM的常规影像及生境分割区域示例和生境体积参数的比较

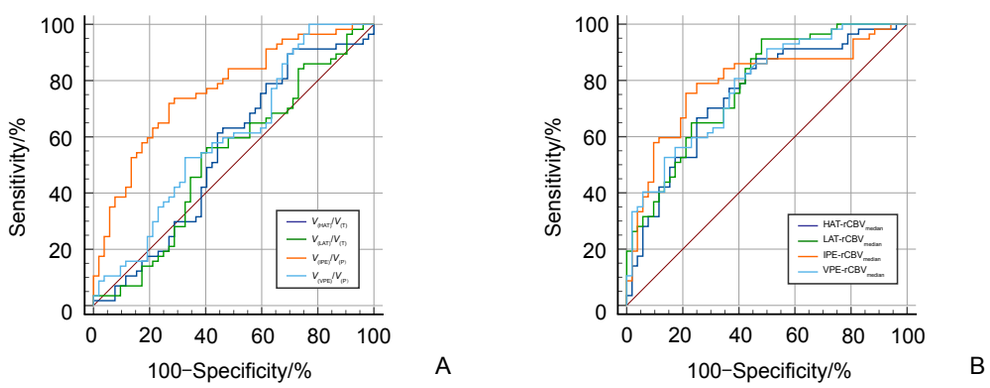
Figure 3 Examples of conventional imaging and habitat segmentation regions, and a comparison of habitat volumetric parameters in GBM and SBM



A~D: Violin plots of the rCBV median values in the HAT, LAT, IPE, and VPE regions for comparison between GBM and SBM. rCBV: Relative cerebral blood volume; HAT: High angiogenic tumor; LAT: Low angiogenic tumor; IPE: Infiltrated peripheral edema; VPE: Vasogenic peripheral edema

图4 GBM和SBM各生境血流参数间的比较

Figure 4 Comparison of hemodynamic parameters among different habitats in the GBM group and SBM group



A: ROC curve of volumetric parameters for discriminating GBM from SBM. B: ROC curve of hemodynamic parameters for discriminating GBM from SBM. rCBV: Relative cerebral blood volume; HAT: High angiogenic tumor; LAT: Low angiogenic tumor; IPE: Infiltrated peripheral edema; VPE: Vasogenic peripheral edema

图5 四种生境区域的体积参数和血流参数鉴别GBM与SBM的受试者工作特征曲线

Figure 5 ROC curves for discriminating GBM from SBM using parameters from 4 habitat regions

表3 各生境特征参数诊断效能

Table 3 Diagnostic efficacy of characteristic parameters of various habitats

Factors	AUC (95%*CI*)	Sensitivity (%)	Specificity(%)	Cut-off value
$V_{(HAT)}/V_{(T)}$	0.548(0.449~0.643)	89.47	30.77	0.428
$V_{(LAT)}/V_{(T)}$	0.526(0.428~0.622)	54.39	61.54	0.470
$V_{(IPE)}/V_{(P)}$	0.765(0.674~0.840)	71.93	73.08	0.122
$V_{(VPE)}/V_{(P)}$	0.601(0.502~0.693)	100.00	23.08	0.323
HAT-rCBV$_{median}$	0.751(0.659~0.830)	66.67	75.00	5.346
LAT-rCBV$_{median}$	0.792(0.704~0.864)	75.44	78.85	2.660
IPE-rCBV$_{median}$	0.779(0.689~0.853)	94.74	51.92	1.321
VPE-rCBV$_{median}$	0.778(0.688~0.852)	80.70	61.54	0.422

rCBV: Relative cerebral blood volume; HAT: High angiogenic tumor; LAT: Low angiogenic tumor; IPE: Infiltrated peripheral edema; VPE: Vasogenic peripheral edema

HAT-rCBV$_{median}$间的相关系数分别为0.561(P<0.01)、0.283(P=0.033),呈显著正相关。而在SBM中,IPE-rCBV$_{median}$和VPE-rCBV$_{median}$与HAT-rCBV$_{median}$间的相关系数分别为0.139(P>0.05)、0.125(P>0.05),并没有显示出明显的相关性。具体相关性分析见表4。

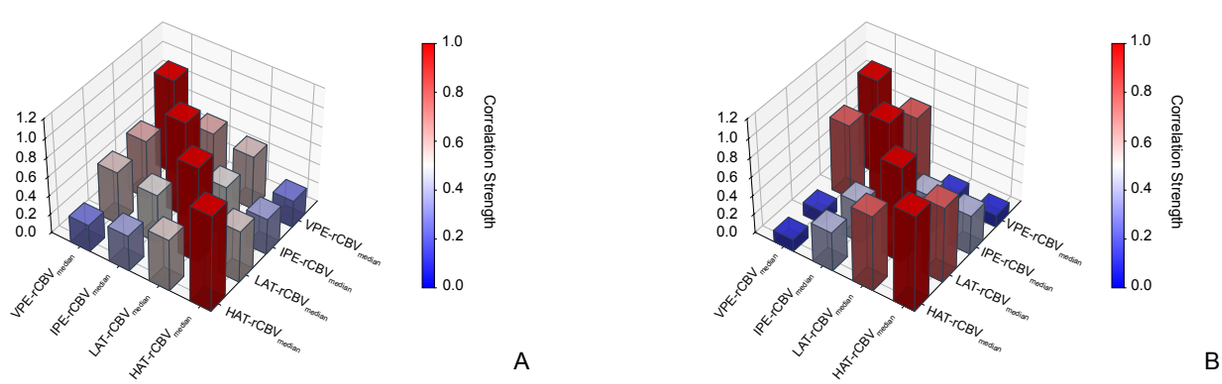
3 讨论

本研究利用DSC-PWI构建肿瘤血管生境,通过生境特征参数对GBM和SBM进行鉴别。研究结果表明,基于DSC-PWI构建的肿瘤血管生境所获得的体积参数$V_{(IPE)}/V_{(P)}$和血流参数rCBV$_{median}$能够作为术前鉴别诊断GBM与SBM的定量参数。

3.1 GBM和SBM生境特征参数间的差异

有研究[9-10]表明,高级别胶质瘤的显著特征之一是瘤周水肿区的扩展,这通常表明肿瘤对邻近脑组织有广泛的侵袭性和破坏,且瘤周水肿区的体积与肿瘤的侵袭性生长高度相关。有研究[11-12]显示,瘤周水肿区的影像组学特征能够有效预测患者胶质瘤复发,且IPE区域作为瘤周水肿区域一部分,其rCBV值可以作为预测高级别胶质瘤局部空间复发模式的影像学标记物。IPE区域在一定程度上反映了肿瘤瘤周水肿区域的异质性,体现了肿瘤浸润性生长区域。而在本研究中,GBM组$V_{(IPE)}/V_{(P)}$显著高于SBM组,这表明在瘤周水肿区域,GBM肿瘤细胞的浸润生长较SBM更为活跃。因此,$V_{(IPE)}/V_{(P)}$不仅在预测胶质瘤复发方面起到重要作用,也能作为鉴别GBM和SBM的一个指标。

ASKANER等[13]研究发现,在常规DSC图像的肿瘤实质强化区,GBM与SBM之间的rCBV值差异无统计学意义,不能作为鉴别诊断的有效指标。然而在本研究中,基于DSC-PWI的肿瘤血管生境分析显示,GBM的四种生境区域中的生境血流参数均高于SBM,且均表现出良好的诊断效能。且有研究[14-15]表明,rCBV反映了肿瘤微血管增生的程度,微血管结构及新生血管增多可导致rCBV值增大。我们的研究结果与其相似,这可能与GBM和SBM肿瘤内部的血管结构、分布及功能状态间的差异有关。



A: Correlation matrix of interactions among hemodynamic parameters in GBM habitats; B: Correlation matrix of interactions among hemodynamic parameters in SBM habitats. In contrast to GBM, where HAT-rCBV$_{median}$ shows significant positive correlations with both IPE-rCBV$_{median}$ and VPE-rCBV$_{median}$, the SBM group shows no significant correlations among these parameters

图6 GBM和SBM组各生境区域作用的比较

Figure 6 Comparison of habitat interactions between the GBM and SBM groups

表4 GBM和SBM组间各生境血流参数的相关性分析

Table 4 Correlation analysis of various habitat hemodynamic parameters between the GBM and SBM groups

Habitat hemodynamic parameters	Correlation coefficient (r) of GBM group	Correlation coefficient (r) of SBM group
HAT-rCBV$_{median}$/LAT-rCBV$_{median}$	0.620[b]	0.785[b]
HAT-rCBV$_{median}$/IPE-rCBV$_{median}$	0.561[b]	0.139
HAT-rCBV$_{median}$/VPE-rCBV$_{median}$	0.283[a]	0.125
LAT-rCBV$_{median}$/IPE-rCBV$_{median}$	0.516[b]	0.426[b]
LAT-rCBV$_{median}$/VPE-rCBV$_{median}$	0.376[b]	0.412[b]
IPE-rCBV$_{median}$/VPE-rCBV$_{median}$	0.542[b]	0.788[b]

a: P<0.05; b: P<0.01

3.2 肿瘤核心区域与瘤周水肿区域间的相互联系

LEMÉE等[16]的研究认为,肿瘤细胞会从肿瘤核心区域向瘤周区域转移。本研究对2类肿瘤生境血流参数相关性分析中,GBM的IPE-rCBV$_{median}$和VPE-rCBV$_{median}$值与HAT-rCBV$_{median}$值具有不同程度的相关性。而SBM的IPE-rCBV$_{median}$和VPE-rCBV$_{median}$值与HAT-rCBV$_{median}$值却并未表现出明显相关性。该结果显示GBM肿瘤实质的异质性与瘤周水肿区域有明确的关联,且一定程度上决定了瘤周区域的异质性,这与LEMÉE等[16]的研究有相似之处。而GBM和SBM中两者表现出的相关性差异也可作为鉴别这2类肿瘤的辅助指标。

3.3 各生境特征参数对GBM和SBM的鉴别诊断价值

本研究中,四个生境区域中的生境血流参数均可以鉴别GBM和SBM。ROC曲线分析显示,在鉴别GBM和SBM时,LAT-rCBV$_{median}$值在全部参数中具有最好的诊断效能,其AUC值为0.794。另外,IPE-rCBV$_{median}$值在鉴别GBM和SBM时,敏感性达到94.74%,能够更准确地识别出GBM患者。同时,本研究还发现GBM组$V_{(IPE)}/V_{(P)}$值高于SBM。以上结果表明两种肿瘤IPE区域的血管异质性存在较大差异,反映了GBM和SBM在肿瘤血管渗漏、水肿形成以及肿瘤微环境调控方面的不同机制,为临床鉴别诊断提供了新的思路。

本研究通过DSC-PWI构建肿瘤血管生境来反映肿瘤的血管异质性,从而对GBM和SBM进行鉴别。目前有学者[17-18]运用平均表观传播扩散MRI(mean apparent propagator-MRI,MAP-MRI)、神经突定向扩散与密度成像(neurite orientation dispersion and density imaging,NODDI)等技术对GBM和SBM鉴别,但结果均不理想。将来的研究可以运用多种成像技术对GBM和SBM进行联合诊断,以期达到更好的诊断效果。而基于多模态MRI构建的生境成像能够更为深入展现肿瘤内部异质性信息[19-21],不仅能够提供肿瘤形态、大小和位置等常规信息,还能够揭示肿瘤微环境的复杂性,在GBM和SBM的鉴别诊断中具有广阔的应用前景。

本研究也存在一定的局限性。首先是本研究为单中心回顾性研究,可能会存在选择性偏倚。其次病例数相对较少,没有进行外部验证。最后是SBM的病理类型不统一,包括肺、胃肠道、卵巢等来源。

综上所述,本研究构建的肿瘤血管生境所获得的生境特征参数rCBV$_{median}$值和$V_{(IPE)}/V_{(P)}$值能够有效鉴别GBM和SBM,为术前无创性鉴别诊断GBM与SBM提供了一种新的思路和方法,并为患者制定后续治疗方案提供一定依据。

利益冲突 本文所有作者声明不存在利益冲突

参考文献:

[1] STUPP R, MASON W P, VAN DEN BENT M J, *et al*. Radiotherapy plus concomitant and adjuvant temozolomide for glioblastoma[J]. N Engl J Med, 2005, 352(10): 987-996. DOI:10.1056/NEJMoa043330.

[2] VOGELBAUM M A, BROWN P D, MESSERSMITH H, *et al*. Treatment for brain metastases: ASCO-SNO-ASTRO guideline[J]. J Clin Oncol, 2022, 40(5): 492-516. DOI: 10.1200/JCO.21.02314.

[3] APARICI-ROBLES F, DAVIDHI A, CAROT-SIERRA J M, *et al*. Glioblastoma versus solitary brain metastasis: MRI differentiation using the edema perfusion gradient[J]. J Neuroimaging, 2022, 32(1): 127-133. DOI: 10.1111/jon.12920.

[4] 李锐, 吴冰, 王玉林, 等. 氨基质子转移成像在鉴别脑内转移瘤和高级别胶质瘤中的应用价值[J]. 第三军医大学学报, 2016, 38(22): 2388-2392. DOI: 10.16016/j.1000-5404.201606132.
LI R, WU B, WANG Y L, *et al*. Application value of amide proton transfer imaging in differential diagnosis of brain metastasis and high grade glioma[J]. J Third Mil Med Univ, 2016, 38(22): 2388-2392. DOI: 10.16016/j.1000-5404.201606132.

[5] PONS-ESCODA A, GARCIA-RUIZ A, NAVAL-BAUDIN P, *et al*. Voxel-level analysis of normalized DSC-PWI time-intensity curves: a potential generalizable approach and its proof of concept in discriminating glioblastoma and metastasis[J]. Eur Radiol. 2022, 32(6): 3705-3715. DOI: 10.1007/s00330-021-08498-1.

[6] HEYNOLD E, ZIMMERMANN M, HORE N, Buchfelder M, *et al*. Physiological MRI Biomarkers in the Differentiation Between Glioblastomas and Solitary Brain Metastases[J]. Mol Imaging Biol. 2021, 23(5): 787-795. DOI: 10.1007/s11307-021-01604-1.

[7] JUAN-ALBARRACÍN J, FUSTER-GARCIA E, PÉREZ-GIEBÉS A, *et al*. Glioblastoma: Vascular Habitats Detected at Preoperative Dynamic Susceptibility-weighted Contrast-enhanced Perfusion MR Imaging Predict Survival[J]. Radiology. 2018 Jun; 287(3): 944-954. DOI: 10.1148/radiol.2017170845.

[8] NAPEL S, MU W, JARDIM-PERASSI B V, *et al*. Quantitative imaging of cancer in the postgenomic era: Radio

(geno)mics, deep learning, and habitats[J]. Cancer, 2018, 124(24): 4633-4649. DOI:10.1002/cncr.31630.

[9] BLYSTAD I, MARCEL WARNTJES J B, SMEDBY Ö, *et al*. Quantitative MRI for analysis of peritumoral edema in malignant gliomas[J]. PLoS One, 2017, 12(5): e0177135. DOI:10.1371/journal.pone.0177135.

[10] TRAN T T, MAHAJAN A, CHIANG V L, *et al*. Perilesional edema in brain metastases: potential causes and implications for treatment with immune therapy[J]. J Immunother Cancer, 2019, 7(1): 200. DOI: 10.1186/s40425-019-0684-z.

[11] 宋珍珍, 孙小玲, 李海鸥, 等. 120例胶质瘤及瘤周水肿MRI影像组学在评估肿瘤复发中的价值[J]. 山东大学学报(医学版), 2021, 59(11): 53-60. DOI:10.6040/j.issn.1671-7554.0.2021.0997.
SONG Z Z, SUN X L, LI H O, *et al*. Value of MRI radiomics of glioma and peritumoral edema in evaluating tumor recurrence[J]. J Shandong Univ Health Sci, 2021, 59(11): 53-60. DOI:10.6040/j.issn.1671-7554.0.2021.0997.

[12] WANG H W, ZENG L L, WU H, *et al*. Preoperative vascular heterogeneity based on dynamic susceptibility contrast MRI in predicting spatial pattern of locally recurrent high-grade gliomas[J]. Eur Radiol, 2024, 34(3): 1982-1993. DOI:10.1007/s00330-023-10149-6.

[13] ASKANER K, RYDELIUS A, ENGELHOLM S, *et al*. Differentiation between glioblastomas and brain metastases and regarding their primary site of malignancy using dynamic susceptibility contrast MRI at 3T[J]. J Neuroradiol, 2019, 46(6): 367-372. DOI: 10.1016/j. neurad. 2018. 09.006.

[14] ÁLVAREZ-TORRES M D M, FUSTER-GARCÍA E, JUAN-ALBARRACÍN J, *et al*. Local detection of microvessels in IDH-wildtype glioblastoma using relative cerebral blood volume: an imaging marker useful for astrocytoma grade 4 classification[J]. BMC Cancer, 2022, 22(1): 40. DOI: 10.1186/s12885-021-09117-4.

[15] 姜新雅, 仇斌, 王维. 星形细胞瘤相对脑血容量与肿瘤血管生成的相关性研究[J]. 中国医学影像技术, 2006, 22(3): 401-404. DOI:10.13929/j.1003-3289.2006.03.028.
JIANG X Y, QIU B, WANG W. Correlation of relative cerebral blood volume with tumor angiogenesis in astrocytomas[J]. Chin J Med Imag Technol, 2006, 22(3): 401-404. DOI:10.13929/j.1003-3289.2006.03.028.

[16] LEMÉE J M, CLAVREUL A, MENEI P. Intratumoral heterogeneity in glioblastoma: don't forget the peritumoral brain zone[J]. Neuro Oncol, 2015, 17(10): 1322-1332. DOI:10.1093/neuonc/nov119.

[17] MAO J J, ZENG W K, ZHANG Q Y, *et al*. Differentiation between high-grade gliomas and solitary brain metastases: a comparison of five diffusion-weighted MRI models[J]. BMC Med Imaging, 2020, 20(1): 124. DOI: 10.1186/s12880-020-00524-w.

[18] KADOTA Y, HIRAI T, AZUMA M, *et al*. Differentiation between glioblastoma and solitary brain metastasis using neurite orientation dispersion and density imaging[J]. J Neuroradiol, 2020, 47(3): 197-202. DOI: 10.1016/j.neurad.2018.10.005.

[19] ZHU Y Y, WANG J, XUE C, *et al*. Deep learning and habitat radiomics for the prediction of glioma pathology using multiparametric MRI: a multicenter study[J]. Acad Radiol, 2025, 32(2): 963-975. DOI: 10.1016/j.acra.2024.09.021.

[20] EUN P, SUNG K, KIM N, *et al*. Spatiotemporal heterogeneity in multiparametric physiologic MRI is associated with patient outcomes in IDH-wildtype glioblastoma[J]. Clin Cancer Res, 2021, 27(1): 237-245. DOI:10.1158/1078-0432.CCR-20-2156.

[21] HYEON M, EUN P, KIM N, *et al*. Prospective longitudinal analysis of imaging-based spatiotemporal tumor habitats in glioblastoma, IDH-wild type: implication in patient outcome using multiparametric physiologic MRI[J]. BMC Cancer, 2024, 24(1): 1197. DOI: 10.1186/s12885-024-12939-7.

(**收稿**:2025-09-30;**修回**:2025-12-25)

(编辑 汤锦波)